Earth and Planetary Science Letters 431 (2015) 264–273

Contents lists available at ScienceDirect

Earth and Planetary Science Letters

www.elsevier.com/locate/epsl

Multiple oscillations in Neoarchaean atmospheric chemistry

Gareth Izon [a,*], Aubrey L. Zerkle [a], Iadviga Zhelezinskaia [b], James Farquhar [b], Robert J. Newton [c], Simon W. Poulton [c], Jennifer L. Eigenbrode [d], Mark W. Claire [a,e]

[a] Department of Earth and Environmental Sciences, University of St Andrews, St Andrews KY16 9AL, Scotland, United Kingdom
[b] Department of Geology and Earth System Science Interdisciplinary Center, University of Maryland, College Park, MD 20742, USA
[c] School of Earth and Environment, University of Leeds, Leeds LS2 9JT, United Kingdom
[d] Solar System Exploration Division, NASA Goddard Space Flight Center, Greenbelt, MD 20771, USA
[e] Blue Marble Space Institute of Science, 1200 Westlake Ave N Suite 1006, Seattle, WA 98109, USA

ARTICLE INFO

Article history:
Received 19 June 2015
Received in revised form 1 September 2015
Accepted 12 September 2015
Available online 4 October 2015
Editor: B. Marty

Keywords:
Neoarchaean
multiple sulphur isotopes
MIF
methane
hydrocarbon haze
atmospheric oxygen

ABSTRACT

The Great Oxidation Event (GOE) represents a crucial juncture in Earth history, signifying the rise in atmospheric oxygen from parts per million to percent levels at ~2.45–2.32 billion-years-ago (Ga). Although planetary oxygenation undoubtedly led to the inception of the contemporary Earth system, the trigger(s) and mechanism(s) controlling this chemical reorganisation remain elusive. Quantitative estimates of the atmosphere's composition in the prelude to the GOE are central to understanding this oxygenation event. Previous analyses of 2.65–2.5 Ga sediments from the Griqualand Basin (South Africa) invoke a tantalising picture of an unusual Earth environment, alluding to an atmosphere periodically dominated by a layer of organic particles ("haze") formed from methane photolysis. However, as yet this hypothesis has remained untested. Here we present four new coupled carbon and quadruple sulphur isotope records from distal, time equivalent (2.7–2.5 Ga), sedimentary successions from South Africa and Western Australia. These extended records reveal similar chemostratigraphic trends, supporting a dynamic terminal-Neoarchaean atmosphere, oscillating between a hazy state at elevated methane concentrations, and a haze-free anoxic background state. We suggest these atmospheric aberrations were related to heightened biogenic methane fluxes fuelled by enhanced nutrient delivery from climatically or weathering induced feedbacks. These data question the canonical view of a simple, unidirectional planetary oxygenation and signify that the overture to the GOE was governed by complex feedbacks within the Earth–biosphere system.

1. Introduction

The early Palaeoproterozoic oxygenation of Earth's surficial environment fundamentally altered the chemistry and ecological structure of our planet. Based on numerous geological and geochemical arguments (e.g., Holland, 2006; Farquhar et al., 2011, 2014), it is widely believed that Archaean atmospheric oxygen was initially low (Pavlov and Kasting, 2002), rising irreversibly to a fraction of present atmospheric levels (PAL) during the GOE (Holland, 2006). Recently, this canonical view of planetary oxygenation has been questioned by analyses of ~3.0–2.5 Ga sediments, which have been interpreted to reflect transient or localised oxygenation (colloquially referred to as "whiffs of oxygen"; Anbar et al., 2007; Wille et al., 2007; Frei et al., 2009; Kendall et al., 2010; Thomazo et al., 2011) as well as periods of more reduced atmospheric composition (Zerkle et al., 2012; Farquhar et al., 2013). Together, these studies hint at a complex atmospheric evolution that we are only beginning to comprehend (e.g., Kurzweil et al., 2013).

The emerging picture of atmospheric evolution is obstructed because most geochemical proxies record oceanic conditions that are only indirectly tied to atmospheric composition. Fortunately, the sedimentary quadruple sulphur isotope record is explicitly linked to the redox state of the atmosphere (e.g., Farquhar et al., 2011; Johnston, 2011; Farquhar et al., 2014), removing some of these uncertainties. The quadruple sulphur isotope record shifts abruptly from mass independent fractionation in the Archaean (S-MIF; $\Delta^{33}S$ and $\Delta^{36}S \neq 0‰$) to mass dependent fractionation in more recent sediments (Fig. 1). The transmittance of S-MIF into the geological record is linked to atmospheric oxygen in multiple ways (see reviews of Farquhar et al., 2011; Johnston, 2011; Farquhar et al., 2014). Firstly, there are only two experimentally verified mechanisms capable of producing large variability

* Corresponding author.
E-mail addresses: gji3@st-andrews.ac.uk, garethjizon@googlemail.com (G. Izon).

http://dx.doi.org/10.1016/j.epsl.2015.09.018

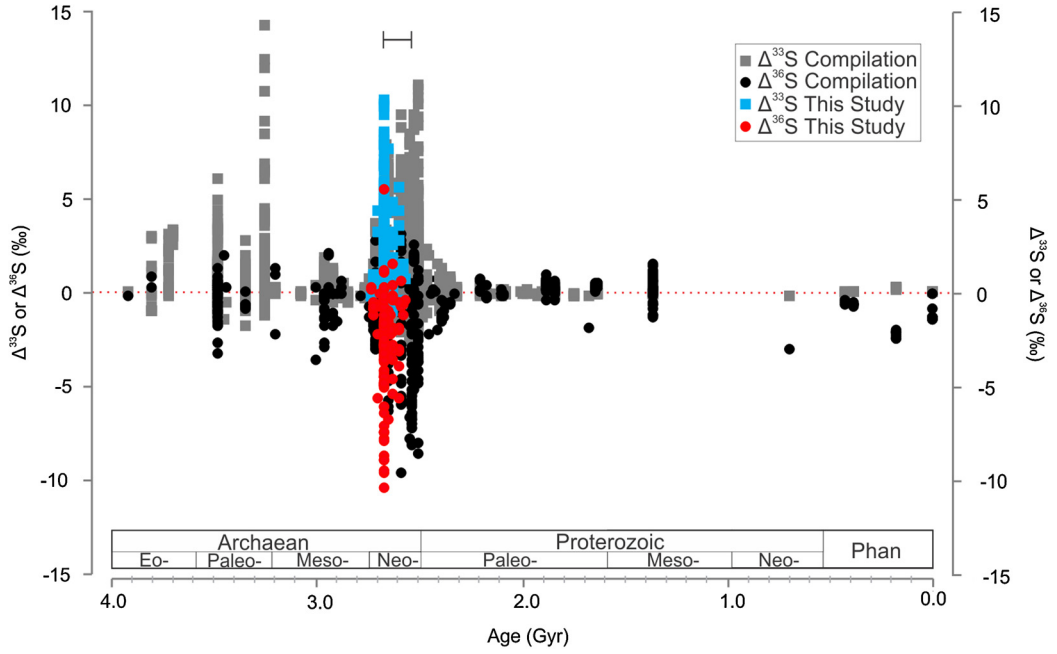

Fig. 1. A temporal compilation of minor S-isotope data. Data are displayed in $\Delta^{3x}S$ notation, as either $\Delta^{33}S$ (squares) or $\Delta^{36}S$ (circles), representing permil (‰) deviations from the terrestrial mass-dependent fractionation line (Equations (2)–(3)). Literature data are updated from Stüeken et al. (2012) after Claire et al. (2014). Compiled $\Delta^{33}S$ and $\Delta^{36}S$ data are given in grey and black symbols, whereas the new data are blue and red respectively. Data from the Hamersley composite record are plotted against age, whereas those from BH1-Sacha are plotted at 2.67 Ga with the horizontal uncertainty representing depositional duration of the core. For interpretation of the references to colour in this figure, the reader is referred to the web version of this article.

in both $\Delta^{33}S$ and $\Delta^{36}S$ that are in agreement with the geological record. These are SO_2 photolysis (Farquhar et al., 2000, 2001; Masterson et al., 2011) and SO_2 photo(de)excitation (Danielache et al., 2012; Whitehill and Ono, 2012; Whitehill et al., 2013). Both processes are atmospheric, the former triggered by the absorption of a photon between 180 and 220 nm yielding SO and O, whereas the second involves excited state SO_2, triggered by photon absorption at longer wavelengths (250–350 nm). Oxygen and ozone, within the contemporary atmosphere, absorb UV radiation throughout these critical wavelengths (180–300 nm), hence precluding any significant tropospheric S-MIF genesis. Contrastingly, the absence of these atmospheric gases effectively removes the tropospheric UV photon shield, permitting short wavelength photon penetration to the lower atmosphere and fuelling S-MIF production (Claire et al., 2014). More subtly, in a reduced atmosphere, sulphur can leave the atmosphere via multiple exit channels at differing redox states (e.g., SO_4, S_8, SO_2), which are homogenised when atmospheric oxygen exceeds 10^{-5} of the present atmospheric level (PAL; Pavlov and Kasting, 2002; Claire et al., 2014). Accordingly, reduced atmospheres further enable sulphur isotopic variability to be generated and transferred to the Earth's surface where it can be preserved. Finally, low-oxygen oceans also increase the likelihood of S-MIF preservation, by permitting the burial of discrete sulphur phases before their isotopic composition can be homogenised and lost (Farquhar et al., 2013; Halevy, 2013).

Once formed, $\Delta^{33}S$ and $\Delta^{36}S$ variations apparently behave as conservative tracers, surviving both long-lived mantle transit (Cabral et al., 2013) and mass dependent hydrothermal alteration (Penniston-Dorland et al., 2008; Kurzweil et al., 2013). Thermochemical sulphate reduction can cause magnetic isotope effects in $\Delta^{33}S$ but not $\Delta^{36}S$ (Oduro et al., 2011b); similarly, biological sulphur cycling can impart small differential effects on $\Delta^{33}S$ and $\Delta^{36}S$ (Ono et al., 2006b), but does not affect $\Delta^{33}S$–$\Delta^{36}S$ covariations (Zerkle et al., 2012). Consequently, non-zero $\Delta^{33}S$ and $\Delta^{36}S$ data from the Archaean is generally interpreted as a primary atmospheric signal, reflecting photochemical production in an atmosphere devoid of significant oxygen. Taken together, these arguments make the presence of S-MIF the most robust evidence for an atmosphere devoid of significant oxygen prior to ~2.45 Ga (Bekker et al., 2004; Guo et al., 2009).

Further interrogation of the Archaean S-MIF record suggests that an additional change in atmospheric chemistry occurred at ~2.7 Ga, marked by a rise in S-MIF magnitude (Fig. 1) and perhaps accompanied by increased propensity toward shallower $\Delta^{36}S/\Delta^{33}S$ slopes (from −1.5 to −0.9; Kurzweil et al., 2013). Initially, a low-magnitude S-MIF signal prior to ~2.7 Ga was interpreted to represent episodic planetary oxygenation (Ohmoto et al., 2006; Ono et al., 2006a); however, this was refuted by $\Delta^{36}S/\Delta^{33}S$ slopes indicative of S-MIF, necessitating a reducing atmosphere (Farquhar et al., 2007). More recently, photochemical simulations have shown that other gases in addition to oxygen can exert a control on S-MIF formation (Domagal-Goldman et al., 2008; Ueno et al., 2009; Zerkle et al., 2012; Claire et al., 2014). Consequently, pre-2.7 Ga muted S-MIF values with apparently steeper $\Delta^{36}S/\Delta^{33}S$ slopes (~ −1.5) were interpreted to reflect a persistent organic haze (Domagal-Goldman et al., 2008; Farquhar et al., 2007; Haqq-Misra et al., 2008) fuelled by photochemical polymerisation of methane derivatives in a reducing atmosphere. At around ~2.7 Ga, S-MIF magnitudes increased, with a concomitant decrease in $\Delta^{36}S/\Delta^{33}S$ slopes to −0.9; an observation interpreted to represent the proliferation of oxygenic photosynthesis, which could have decreased the atmospheric CH_4:CO_2 mixing ratio and cleared the established organic-rich haze (Eigenbrode and Freeman, 2006; Farquhar et al., 2011; Kurzweil et al., 2013).

More recently, periodic changes in $\Delta^{36}S/\Delta^{33}S$ slopes preserved in Neoarchaean sediments were suggested to represent a bi-stable atmosphere, oscillating between a haze-free anoxic background and an organic-rich hazy state (Zerkle et al., 2012). This hypothesis was based on analyses from a single core (GKF01; Fig. 2) through the ~2.65–2.5 Ga Ghaap Group (Griqualand West Basin, Transvaal Supergroup, South Africa), which revealed co-variation between the minor isotopes of sulphur preserved in pyrite and the carbon isotopic composition of synchronous organic matter

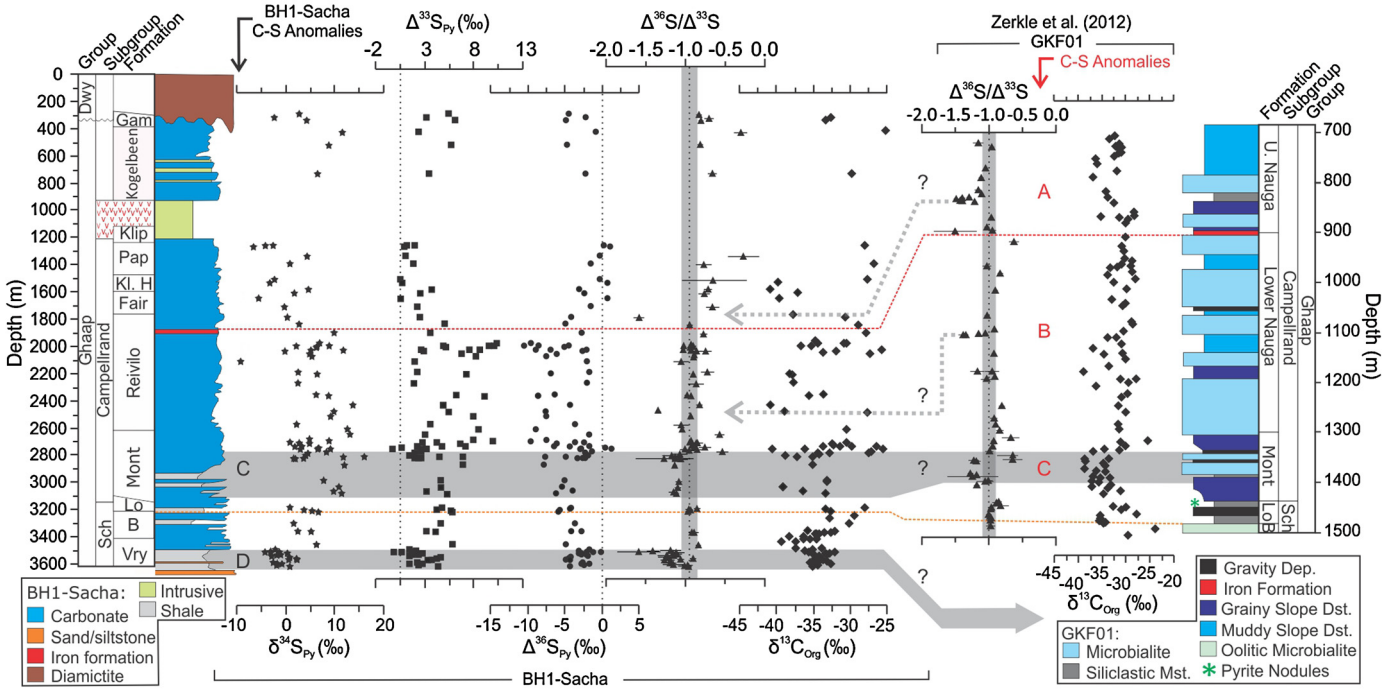

Fig. 2. Lithological and geochemical data for both BH1-Sacha and GKF01 (Zerkle et al., 2012) plotted against core depth (m). These data sets are correlated based on the position of a flooding surface at the top of the Boomplaas Formation (lower orange dashed line) and the Kamden Member iron formation within the Reivilo/Lower Nauga Formation (upper red dashed line; Fischer et al., 2009). Chronological constraints on these datums are based on SHRIMP U–Pb zircon ages summarised in Knoll and Beukes (2009). Data from BH1-Sacha include pyrite S-isotope values ($\delta^{34}S$, $\Delta^{33}S$, $\Delta^{36}S$), $\Delta^{36}S/\Delta^{33}S$ and the carbon isotopic composition of organic residues ($\delta^{13}C_{Org}$). Complementary $\Delta^{36}S/\Delta^{33}S$ and $\delta^{13}C_{Org}$ are shown from GKF01 (Zerkle et al., 2012) and the initially identified C–S anomalies are labelled A–C. Vertical dashed lines on $\Delta^{36}S/\Delta^{33}S$ plots signify the average slope of the dataset (Fig. 3A), whereas the grey vertical envelope corresponds to $\pm$ 0.1 uncertainties after Zerkle et al. (2012). Horizontal grey bands denote identified C–S anomalies, whereas dotted arrows signify single data points showing increased $\Delta^{36}S/\Delta^{33}S$ and decreased $\delta^{13}C_{Org}$ (see text for discussion). Abbreviations: Sch, Dwy, Vry, B, Lo, Mont, Fair, Kl. H, Pap, Klip and Gam represent Schmidtsdrif, Dwyka, Vryburg, Boomplaas, Lokammona, Monteville, Fairfield, Klipfontein Heuwel, Papkuil, Klippan and Gamohaan respectively. For interpretation of the references to colour in this figure, the reader is referred to the web version of this article.

($\delta^{13}C_{Org}$; Intervals A–C, Fig. 2; Zerkle et al., 2012; Farquhar et al., 2013). Specifically, this record showed changes in the $\Delta^{36}S/\Delta^{33}S$ slopes (steepening from -0.9 to -1.5) over restricted stratigraphic intervals characterised by ^{13}C-depleted organic matter ($\delta^{13}C_{Org} \leq -37‰$). Depletions in $\delta^{13}C_{Org}$ of this magnitude are typically interpreted to reflect increased incorporation of ^{13}C-depleted substrates (i.e., methane) into sedimentary matter following enhanced methanogenesis and methanotrophy (e.g., Eigenbrode and Freeman, 2006; Zerkle et al., 2012; Thomazo et al., 2013). Regardless of the mechanism of preserving ^{13}C-depleted carbon (cf., Pavlov et al., 2001), these data imply a link between S-MIF producing atmospheric chemistry and enhanced methane availability in the Earth–atmosphere system. One-dimensional photochemical models corroborate this inferred link, predicting that at elevated CH_4:CO_2 mixing ratios a hydrocarbon haze is formed (Pavlov et al., 2001), which could alter S-MIF by either shielding S-MIF-forming reactions or altering their relative importance (Domagal-Goldman et al., 2008; Zerkle et al., 2012; Kurzweil et al., 2013; Claire et al., 2014).

Crucially, if the Neoarchean were associated with the periodic development of a globally extensive atmospheric hydrocarbon haze governing S-MIF formation then we would expect similar correlations in coupled carbon- and sulphur-isotope records to be spatially widespread and temporally correlative. To test this 'haze' hypothesis, we produced four new coupled quadruple sulphur ($\delta^{34}S$, $\Delta^{33}S$ and $\Delta^{36}S$) and $\delta^{13}C_{Org}$ records from time equivalent sections spanning the Griqualand West Basin (BH1-Sacha; Fischer et al., 2009; Alterman and Siegfried, 1997) and from the Hamersley Province in Western Australia (Eigenbrode and Freeman, 2006; Czaja et al., 2010).

2. Geological setting and core materials

2.1. The Griqualand West Basin

The Archaean–Palaeoproterozoic Transvaal Supergroup is exceptionally well preserved in the Griqualand West Basin, South Africa, generally displaying little tectonic deformation (Beukes, 1987; Eriksson et al., 2006; Sumner and Beukes, 2006). Importantly, significant metamorphic overprinting is restricted to strata in proximity to the Bushveld Igneous Province, with the remainder of the lower Transvaal Supergroup suffering only sub-greenschist facies metamorphism (Button, 1973; Miyano and Beukes, 1984).

We have generated a coupled carbon- and sulphur-isotope record from an additional core drilled from the same sedimentary basin as that used by Zerkle et al. (2012), BH1-Sacha (Altermann and Siegfried, 1997; Altermann and Nelson, 1998; Fischer et al., 2009). Here we concentrate on the lower volcano-sedimentary Ghaap group (Schmidtsdrif–Campbellrand Subgroup; Eriksson et al., 2006), which represents the development of a mixed siliciclastic-carbonate ramp (Schmidtsdrif Subgroup) overlain by an extensive carbonate platform (Campbellrand Subgroup; Altermann and Nelson, 1998; Altermann and Siegfried, 1997; Beukes, 1987; Eriksson et al., 2006). Additionally, a number of igneous intrusive bodies were recovered in BH1-Sacha. No analyses of banded iron formations, igneous lithologies or their metamorphosed counterparts are presented here. Instead we focus our analyses on siliciclastic and carbonate sedimentary units.

Throughout the Griqualand West Basin the Schmidtsdrif Subgroup is composed of mixed siliciclastic and carbonate units whose maximum depositional age is inferred to be between 2.642 $\pm$ 0.003 Ga and 2.664 $\pm$ 0.001 Ga (Fischer et al., 2009). The over-

lying Campbellrand Subgroup displays spatial heterogeneity within the Griqualand West Basin, resulting from the basinal configuration and the paleowater depth, with shallow water facies (Ghaap Plateau) restricted to the north of Griquatown Fault Zone and the deeper water facies equivalents (Prieska) to the south (Altermann and Siegfried, 1997; Eriksson et al., 2006; Fischer et al., 2009; Sumner and Beukes, 2006). Consequently, BH1-Sacha records Ghaap Plateau type sedimentation, which extends laterally into the deeper Prieska facies recorded by GKF01 (Fischer et al., 2009; Zerkle et al., 2012).

The depositional age of the Campbellrand Subgroup is predominantly constrained by SHRIMP U–Pb analyses derived from zircons concentrated from the various intercalated tuff beds (Knoll and Beukes, 2009). In the basinal facies, an age of 2.650 ± 0.008 Ga was reported from the Lokammona Formation (upper Schmidtsdrif Subgroup), with ages of 2.602 ± 0.014 Ga in lower part of the Nauga Formation, 2.581 ± 0.009 Ga immediately below the Kamden Member, and numerous statistically indistinguishable ages of *c*. 2.560 Ga in the upper Nauga Formation (Knoll and Beukes, 2009). These ages compare favourably with those published from the Ghaap Plateau equivalents, with reported ages of 2.555 ± 0.019 Ga from the upper Monteville Formation (Altermann and Nelson, 1998) and two statistically indistinguishable ages of 2.521 ± 0.003 Ga and 2.516 ± 0.004 Ga (Altermann and Nelson, 1998) from the upper Gamohaan Formation.

2.2. The Hamersley composite record

The second set of coupled carbon- and sulphur-isotope records were constructed from three cores collected from the ~2.77–2.43 Ga sedimentary-igneous Mount Bruce Megasequence Set preserved within Hamersley Province, Pilbara Craton. Mineral assemblages show that the Hamersley Basin has also experienced relatively low-grade metamorphism, remaining below greenschist grade (Smith et al., 1982). Moreover, observations from the studied cores lack evidence for large-scale redistribution of sulphur by either secondary pyritisation or post-depositional fluid flow (Czaja et al., 2010), evidenced by the $\delta^{18}O$ composition of carbonates, which approximate those of unaltered Neoarchaean carbonates (Czaja et al., 2010; Eigenbrode and Freeman, 2006).

In this record we utilised three cores from two separate regions of the Hamersley Province, with the first two cores (WRL1, SV1) obtained from the centre of the paleobasin ("main outcrop area"), both within the depocenter (WRL1) and ~60 km to the NNW (SV1; Meakins, 1987; Czaja et al., 2010). The remaining core, RHDH2a, was drilled in the east-northeast part of the province ("Oakover River area"). The depositional histories of both the main outcrop area (Blake, 1993; Blake et al., 2004; Blockley et al., 1993; Lascelles, 2000; Thorne and Trendall, 2001; Trendall and Blockley, 1970; Czaja et al., 2010) and the Oakover River area (Simonson et al., 1993; Eigenbrode and Freeman, 2006; Czaja et al., 2010) have been detailed previously; whereas the specific sedimentology of WRL1, SV1, and RHDH2a cores was detailed by Meakins (1987), Lawrence (1985), and Richards (1985) and precised further by Eigenbrode and Freeman (2006) and Czaja et al. (2010). To correlate across the ~300 km of the province and construct our Hamersley composite record, we applied the chronostratigraphic model described by Eigenbrode and Freeman (2006) and Czaja et al. (2010), who exploited synchronous impact spherule layers, geochronological data and intergraded depositional rates.

3. Analytical methods

The BH1-Sacha core was sampled at the National Core Library at Donkerhoek (Pretoria, South Africa). The samples from Western Australia were supplied from previous sampling of cores that are no longer available (as described in Eigenbrode and Freeman, 2006; Eigenbrode et al., 2008; Czaja et al., 2010).

Sulphide phases were extracted from sediments for isotope analyses via sequential reflux with 6M HCl followed by acidified 1M $CrCl_2$ (Canfield et al., 1986) and precipitated as pure silver sulphide (Ag_2S). Isotope analyses of the Ag_2S were conducted at the University of Maryland, via fluorination, cryogenic purification and dual-inlet isotope ratio mass spectrometry (DI-IRMS) following well-established methodologies (e.g., Oduro et al., 2011a; Zerkle et al., 2012). Analytical external uncertainties on S-isotope measurements are estimated from long-term reproducibility of Ag_2S fluorinations, and are deemed to be 0.02, 0.008, and 0.20‰ (1 standard deviation, 1σ) for $\delta^{34}S$, $\Delta^{33}S$, and $\Delta^{36}S$ ratios, respectively (Zerkle et al., 2012). The accuracy of the presented data was assessed using IAEA S1 and S3 standards, producing data inline with published accepted values.

Sulphur-isotope ratios are reported using delta (δ) notation, reflecting the permil (‰) deviation of the sample composition from that of an international reference standard (Vienna Canyon Diablo Troilite; V-CDT; Equation (1)). Mass independent fractionation is quantified in capital-delta (Δ) notation and is a measure of the ‰ departure from the expected mass-dependent fractionation line (Equations (2)–(3)). The uncertainties on $\Delta^{36}S/\Delta^{33}S$ ratios are computed from the larger of the internal or external uncertainties for $\Delta^{36}S$ and $\Delta^{33}S$, resulting in larger uncertainties associated with smaller magnitude S-MIF (Figs. 2–4), governed predominantly by the raw $\Delta^{36}S$ data.

$$\delta^{34}S = \left(\frac{(^{34}S/^{32}S)_{sample}}{(^{34}S/^{32}S)_{V\text{-}CDT}}\right) - 1 \quad (1)$$

$$\Delta^{33}S = \frac{(^{33}S/^{32}S)_{sample}}{(^{33}S/^{32}S)_{V\text{-}CDT}} - \left[\frac{(^{34}S/^{32}S)_{sample}}{(^{34}S/^{32}S)_{V\text{-}CDT}}\right]^{0.515} \quad (2)$$

$$\Delta^{36}S = \frac{(^{36}S/^{32}S)_{sample}}{(^{36}S/^{32}S)_{V\text{-}CDT}} - \left[\frac{(^{34}S/^{32}S)_{sample}}{(^{34}S/^{32}S)_{V\text{-}CDT}}\right]^{1.9} \quad (3)$$

Samples were prepared for carbon-isotope determination via triplicate overnight 10% (vol/vol) HCl acid rinses to liberate carbonate-carbon. Calcium carbonate ($CaCO_3$) abundance was calculated gravimetrically, assuming that the mass lost due to CO_2 release was all carbonate. Sediment residues were then homogenised and their $\delta^{13}C_{Org}$ determined using a vario Pyro cube interfaced with an Isoprime mass spectrometer forming a continuous flow EA-IRMS system at the University of Leeds, UK. Carbon-isotope data are expressed as permil deviations from the Vienna-PeeDee Belemnite (v-PDB) standard (Equation (4)).

$$\delta^{13}C = \left(\frac{(^{13}C/^{12}C)_{sample}}{(^{13}C/^{12}C)_{V\text{-}PDB}}\right) - 1 \quad (4)$$

Calibration was achieved using IAEA-CH-7, and an in-house sucrose with assigned values of −31.83 and −12.10‰ respectively. Precision on samples was better than 0.3‰, calculated from bracketing standards. Sulphur- and C-isotope data from each record are tabulated in the online supplementary material.

4. Results

4.1. The Griqualand West basin

Carbon- and S-isotope data from BH1-Sacha vary considerably up-core (Figs. 2–3). All the analysed samples display S-MIF, with $\Delta^{33}S$ values between −0.3‰ and 10.4‰, centred on a mean of 4.0 ± 2.5‰ (1σ, here and throughout), and $\Delta^{36}S$ between −10.4‰ and 5.6‰, displaying a mean of −3.6 ± 2.8‰. Major sulphur-isotope data ($\delta^{34}S$; Fig. 2) approximate those reported from GKF01,

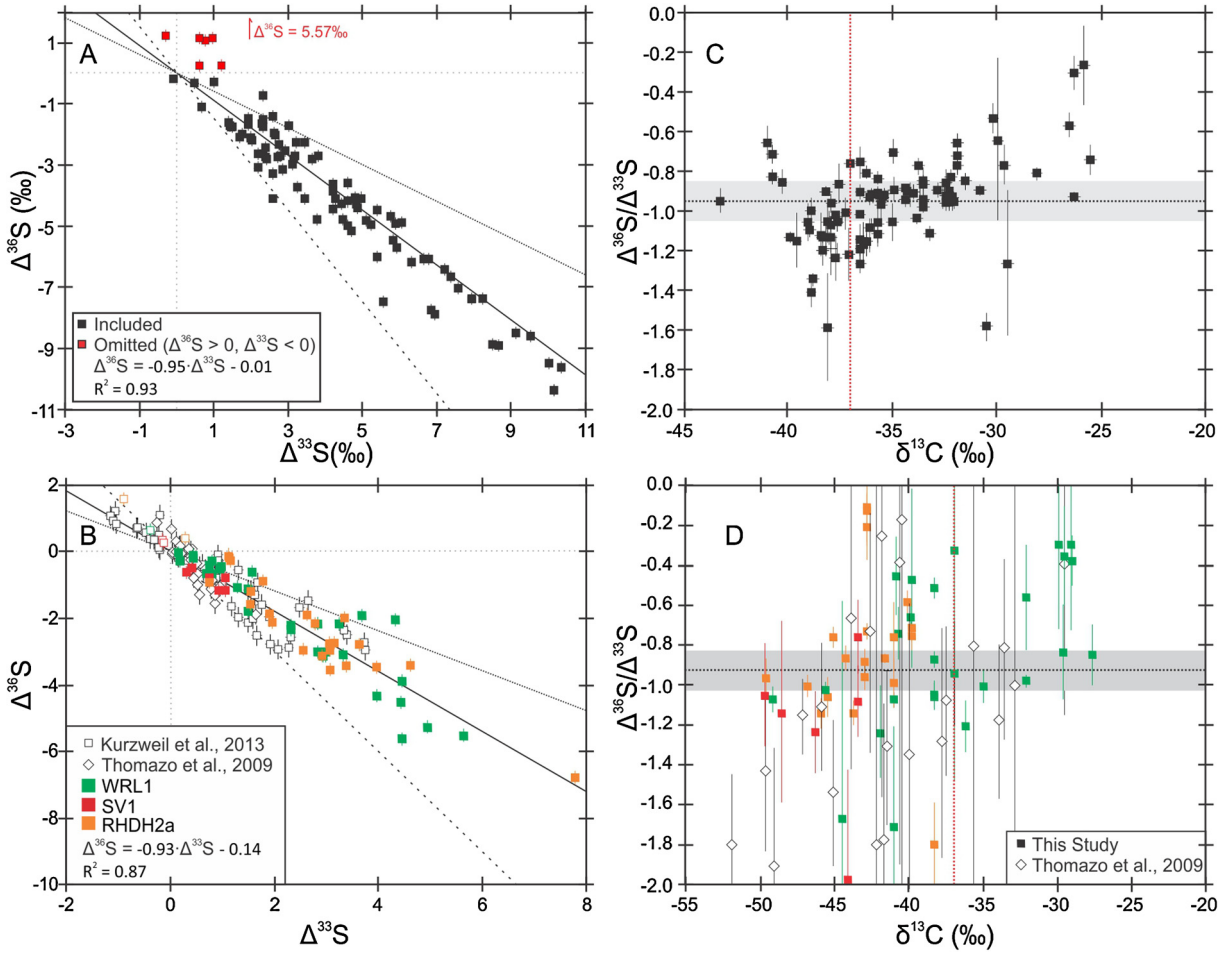

Fig. 3. Quadruple sulphur-isotope data ($\Delta^{33}S$ versus $\Delta^{36}S$) derived from BH1-Sacha (**A**) and the Hamersley composite record **(B)**. Linear fits are given after removing data whose $\Delta^{36}S$ exceeds 0 and $\Delta^{33}S$ is less than 0. The black dotted, solid and dashed lines in parts **A** and **B** signify $\Delta^{36}S/\Delta^{33}S$ slopes of −0.6, −0.9 and −1.5 respectively. Data from the Hamersley composite record are derived from three cores, which are designated by colour (**B** and **D**) and are supplemented by additional data from the 2.73 Ga Tumbiana Formation (open diamonds; Thomazo et al., 2009; **B** and **D**) and 2.71 Kid Creek Formation (open squares Kurzweil et al., 2013; **B**). Quadruple sulphur-isotope ($\Delta^{36}S/\Delta^{33}S$) data versus carbon-isotope data ($\delta^{13}C_{Org}$) for BH1-Sacha **(C)** and the Hamersley composite record **(D)**. Error bars represent the larger of the propagated internal or external analytical uncertainly on $\Delta^{36}S/\Delta^{33}S$ ratios, which are primarily a function of the magnitude of the raw $\Delta^{36}S$ data used to compute them. Horizontal black dotted lines and their grey envelopes signify the average slope of each dataset ±0.1 in parts **C** and **D**, whereas the red vertical dashed lines signify $\delta^{13}C_{Org}$ of $< -37‰$. For interpretation of the references to colour in this figure, the reader is referred to the web version of this article.

ranging from −9.3 to 15.9‰, with an average of 3.6 ± 5.2‰. Finally, carbon-isotope data range from −44.4 to −20.6‰, averaging −33.9 ± 5.1‰, displaying short-term variability.

Closer examination of the data from BH1-Sacha demonstrates that the majority of samples form a linear array in $\Delta^{36}S$–$\Delta^{33}S$ isotope space, with an average $\Delta^{36}S/\Delta^{33}S$ slope of −0.95 (Fig. 3A), closely approximating both the general Neoarchaean reference array (−0.90; Ono et al., 2003) and those reported from GKF01 (−0.96; Zerkle et al., 2012). Significantly, there are a number of samples which deviate from those predicted by the $\Delta^{36}S = -0.95 \times \Delta^{33}S$ linear array, featuring $\Delta^{36}S/\Delta^{33}S$ ratios between ∼−0.60 and −1.5. Samples with divergent $\Delta^{36}S/\Delta^{33}S$ ratios (i.e., $\neq -0.95 \pm 0.1$) are not randomly distributed, but appear to be clustered in distinct stratigraphic intervals (Fig. 2). Consequently, from our BH1-Sacha record we are able to identify potentially two intervals where $\Delta^{36}S/\Delta^{33}S$ ratios become systematically more negative ("steep" $\Delta^{36}S/\Delta^{33}S$ slopes < -1.05; C–D, Fig. 2), with an additional two tentative intervals defined by single data points (dotted arrows, Fig. 2). There are also a number of samples that display less negative $\Delta^{36}S/\Delta^{33}S$ ratios than predicted by the reference array (i.e., "shallow" $\Delta^{36}S/\Delta^{33}S$ slopes > -0.85; Fig. 3A). Although more prevalent in BH1-Sacha, these intervals of shallow slopes are also observed in core GKF01; however, they were previously masked by the absolute value component of the $\Delta^{36}S/\Delta^{33}S_{DEV}$ metric employed by Zerkle et al. (2012).

The intervals of steep $\Delta^{36}S/\Delta^{33}S$ slopes (C–D) in BH1-Sacha are broadly correlative with intervals of ^{13}C-depleted organic matter ($\delta^{13}C_{Org} < -37‰$), hereafter termed "C–S anomalies". Two additional data-points hint at the same correlation, but occur in regions where our core sampling was sparse (Fig. 2). Fig. 4C confirms the correlation between steep $\Delta^{36}S/\Delta^{33}S$ slopes and negative $\delta^{13}C_{Org}$. With the exception of one data point at 1790 m, samples with steep $\Delta^{36}S/\Delta^{33}S$ (< -1.1) correspond to $\delta^{13}C_{Org}$ around −37‰. Contrastingly, samples with shallow $\Delta^{36}S/\Delta^{33}S$ (> -0.9) define two populations: those corresponding to extremely negative $\delta^{13}C_{Org}$ ($< -40‰$) and those that display relatively ^{13}C-enriched $\delta^{13}C_{Org}$ ($> -30‰$). Stratigraphically, the first of these populations ($\Delta^{36}S/\Delta^{33}S > -0.85$, $\delta^{13}C_{Org} < -40‰$) are distributed as isolated data points below 1580 m, whereas the second population ($\Delta^{36}S/\Delta^{33}S > -0.85$, $\delta^{13}C_{Org} > -30‰$) seems to be concentrated in the upper part of the record (Fig. 2).

The Griqualand West basin contains two robust lithological and sequence stratigraphic markers, the Boomplaas flooding surface and the Kamden member iron formation (Fig. 2), that can be used to compare isotope records between our new BH-1 Sacha data and that from GKF01 (Altermann and Siegfried, 1997;

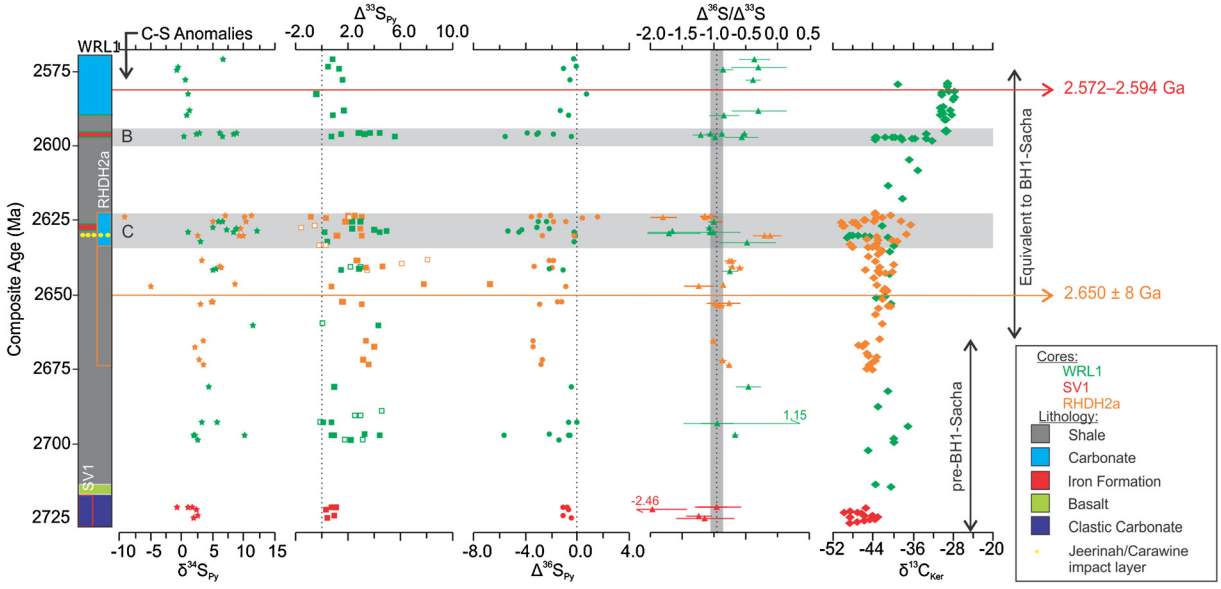

Fig. 4. Lithological, $\delta^{34}S$, $\Delta^{33}S$, $\Delta^{36}S$, $\Delta^{36}S/\Delta^{33}S$ and $\delta^{13}C_{Org}$ data from the Hamersley composite record plotted against age. New data are derived from three cores, designated by different coloured symbols. Existing $\delta^{13}C_{Org}$ data were sourced from Eigenbrode and Freeman (2006) and additional $\Delta^{33}S$ from Ono et al. (2003; open symbols). Correlation with the South African records is based on existing radiometric age constraints on the Boomplass flooding surface (lower, orange line) and the Kamden Member iron formation (upper, red line). Vertical black dotted lines and their grey envelopes on the $\Delta^{36}S/\Delta^{33}S$ plots signify the average slope of each dataset ±0.1 (Fig. 4B), whereas horizontal grey bands (B–C) represent C–S anomalies and are discussed in the text. For interpretation of the references to colour in this figure, the reader is referred to the web version of this article.

Schröder et al., 2006). These datums, to a first order, provide two stratigraphic tie-points to examine our S-isotope data and the synchrony of the identified C–S anomalies (Fischer et al., 2009). Within this simple stratigraphic-framework, we identify a single C–S anomaly (C) between the two sequence stratigraphic datums and one below (D). While C–S anomaly D corresponds to strata that apparently predate GKF01, anomaly C bares a striking structural similarity to the oldest C–S anomaly in GKF01, and its stratigraphic position is consistent with them being potentially correlative (Fig. 2). Within the resolution of the BH1-Sacha record we are unable to confidently identify any further C–S anomalies that may correspond to the younger interval (A, Fig. 2) identified by Zerkle et al. (2012). Nevertheless, we do note single data points in the appropriate stratigraphic position that feature steep $\Delta^{36}S/\Delta^{33}S$ slopes and appropriately low $\delta^{13}C_{Org}$ (dotted arrows, Fig. 2). The upper C–S anomalies in the GKF01 record occur over restricted stratigraphic intervals (<20 m); it was unfortunately beyond the realm of the present study to sample the >3 km long BH1-Sacha core at higher resolution intervals. However, the data from this study will be crucial in informing future higher-resolution sampling necessary to reveal the true structure and frequency of these chemostratigraphic trends.

4.2. The Hamersley record

Like the South African records, the Hamersley record is dominated by S-MIF, with $\Delta^{33}S$ values between −0.89‰ and 7.77‰ with an average of 2.1 ± 1.7‰, values of $\Delta^{36}S$ between −6.75‰ and 1.60‰ with an average of −1.8 ± 1.7‰, and $\delta^{34}S$ values ranging from −9.0 to 12.2‰ with an average of 4.5 ± 4.0‰. The C-isotope data from the Hamersley composite record has been published previously (Eigenbrode and Freeman, 2006) but briefly shows ∼15‰ systematic increase in $\delta^{13}C_{Org}$, with periodic and pronounced negative excursions superimposed on this evolving background.

Despite the persistence of S-MIF, the magnitude of $\Delta^{33}S$ and $\Delta^{36}S$ shows more variability than its South African counterpart. Here, low magnitude S-MIF (< ± 2‰) is observed in the lowest part of the Hamersley record (the Tumbiana Formation), while magnitudes increase in younger sediments. As within the Griqualand West basin, it is possible to identify intervals in the Hamersley record (intervals B–C, Fig. 4) that have $\Delta^{36}S/\Delta^{33}S < -1.0$ (Fig. 3B). Fig. 4 reveals that these slope changes are stratigraphically restricted; one in particular is broadly synchronous between two age-equivalent cores (Interval C, Fig. 4) cores WRL1 and RHDH2a) and each corresponds to negative inflections in $\delta^{13}C_{Org}$ record. Despite the large uncertainty associated with determining slopes from small magnitude S-MIF, some samples from the Tumbiana Formation (red points on Figs. 3D–4) display steep $\Delta^{36}S/\Delta^{33}S$ (< −0.9).

Radiometric age constraints on the Boomplaas flooding surface and the Kamden member iron formation facilitate comparison between the South African cores and the Hamersley composite record (Fig. 4). In the upper part of the Hamersley record, we identify two C–S anomalies (B–C) that occur between these sequence-stratigraphic datums, with a lower more diffuse anomaly and younger more abrupt anomaly, a similar structure to those in the GKF01 record. However, the youngest C–S anomaly preserved in GKF01 (A) and the oldest C–S anomaly preserved in BH1-Sacha (D) are not evident in our sparse sampling of the Hamersley composite record.

With exception of the identified C–S anomalies and some samples from the Tumbiana Formation, the bulk of the Hamersley record comprises fairly shallow $\Delta^{36}S/\Delta^{33}S$ slopes (i.e., > −0.83). In detail, these shallow $\Delta^{36}S/\Delta^{33}S$ slopes do not seem to define the two separate populations seen in the BH1-Sacha record when considered on $\Delta^{36}S/\Delta^{33}S$-$\delta^{13}C_{Org}$ cross-plots (Fig. 3C–D); instead, these samples occupy the complete spectrum of $\delta^{13}C_{Org}$ (*c.* 30–50‰).

5. Discussion

The initial notion of a periodically hazy Neoarchean atmosphere was based on an observed relationship between steep $\Delta^{36}S/\Delta^{33}S$ slopes (< −1.0) and ^{13}C-depleted organic carbon from a single core (Zerkle et al., 2012). To test this 'haze' hypothesis, we produced four new coupled quadruple sulphur and $\delta^{13}C_{Org}$ records

from time equivalent sections, in order to search for similar isotopic covariation — a corollary of the "haze" hypothesis. These new records extend across the Griqualand West basin in South Africa and into the Hamersley Province, Western Australia, providing, for the first time, a definitive intra- and inter-basinal test of the 'haze' hypothesis.

In line with the haze hypothesis, our new data show widespread spatial distribution of steep $\Delta^{36}S/\Delta^{33}S$ slopes correlated with ^{13}C-depleted organic carbon, indicating a change in S-MIF forming reactions in association with enhanced methane production. Moreover, the application of sequence stratigraphic and radiometric correlations reveals that a number of these C–S anomalies are likely synchronous, further supporting a periodic change in global atmospheric state towards hazy conditions. Importantly, these new data hint at as many as 4 distinct C–S anomalies, suggesting that the Neoarchean atmosphere was even more dynamic than previously recognised. Intriguingly, these records also reveal a periodic correspondence between ^{13}C-enriched C and shallow $\Delta^{36}S/\Delta^{33}S$ slopes in both the Hamersley and BH1-Sacha records, which could represent a secondary, previously unrecognised change in atmospheric evolution independent of haze production (e.g. Oduro et al., 2014).

In the following discussion we seek to integrate our new observations with mathematical models and existing hypotheses to elucidate our understanding of atmospheric evolution and speculate on the drivers of this change in the prelude to the GOE.

5.1. Synthesis and implications for the evolution of atmospheric chemistry: integrating mathematical models and geochemical data

Our new S-MIF records focus predominantly on the ~250 million years preceding the GOE, but overlap with some older sediments to which similar 'hazy' interpretations have been applied (e.g., Thomazo et al., 2009). Previous authors have documented a shallowing in $\Delta^{36}S/\Delta^{33}S$ slopes from −1.5 in Tumbiana age (2.73 Ga) strata to −0.9 in 2.71 Ga Kid Creek (Ontario, Canada) sediments. This change is slope is only marginally borne out via statistical analysis of $\Delta^{36}S/\Delta^{33}S$ slope trends (Johnston, 2011) but has been interpreted as a major rearrangement in atmospheric chemistry at ~2.73–2.71 Ga (Kurzweil et al., 2013). The Tumbiana Formation, which forms the basal part of our Hamersley composite record, shows low magnitude $\Delta^{33}S$ and $\Delta^{36}S$ that plot in proximity to the origin in $\Delta^{36}S/\Delta^{33}S$ three-isotope space (Fig. 3B). Our new data, along with closer scrutiny of others (Fig. 3B; Thomazo et al., 2009; Farquhar et al., 2007), appears inconsistent with the claim of a constant $\Delta^{36}S/\Delta^{33}S$ slope of −1.5 for the Tumbiana Formation. This is primarily due to the intrinsic uncertainties in calculating $\Delta^{36}S/\Delta^{33}S$ slopes at low magnitude S-MIF, especially given measurement uncertainties of ~0.2‰ on $\Delta^{36}S$. Notably, propagating this analytical error into the calculation of slope leads to difficulties in precisely defining slopes when S-MIF magnitudes are smaller, as evidenced by the larger error bars on the Tumbiana $\Delta^{36}S/\Delta^{33}S$ samples in Fig. 3D compared to those in Fig. 3C. While we question the occurrence of *uniformly* steep $\Delta^{36}S/\Delta^{33}S$ slopes in the Tumbiana, the data do *periodically* attain steep slopes at low S-MIF magnitude, implying that previous interpretations of Mesoarchaean atmospheric chemistry may be at least partially correct (cf. Kurzweil et al., 2013).

Under a strongly reducing atmosphere prior to any significant O_2 flux from oxygenic photosynthesis (e.g., Kasting et al., 2001; Pavlov et al., 2001), photochemical models predict that atmospheric sulphur removal would have been dominated by the S_8 exit channel (Pavlov and Kasting, 2002). If the majority of sulphur exited the atmosphere via one dominant vector, that species will naturally feature lower magnitude S-MIF following mass balance constraints (Kurzweil et al., 2013; Claire et al., 2014). Consequently, the low magnitude S-MIF signal preserved within the Tumbiana Formation can be potentially reconciled by the dominance of the S_8 exit channel at very low oxygen concentrations, augmented by a larger total sulphur flux and/or hazy atmospheric conditions (Francisco et al., 2005; Ono et al., 2009; Kurzweil et al., 2013; Claire et al., 2014).

The extremely low $\delta^{13}C_{Org}$ preserved in the 2.73 Ga Tumbiana Formation directly precedes the increased magnitude S-MIF signals in temporal records (Fig. 1; Eigenbrode and Freeman, 2006; Thomazo et al., 2009; Fig. 4). Such ^{13}C-depleted $\delta^{13}C_{Org}$ values can only be explained by prevalent methanotrophic activity, which implies widespread methanogenesis leading to increased environmental availability of methane. Elevated methane concentrations are fully consistent with an interpretation involving an organic haze at elevated atmospheric CH_4:CO_2 mixing ratios (e.g., Pavlov et al., 2001), although it must be acknowledged that discrimination between specific gas compositions, beyond the absence of oxygen and ozone, is not yet feasible with current predictive models (Claire et al., 2014) and is the subject of on-going work.

In sediments younger than ~2.7 Ga, $\delta^{13}C_{Org}$ is observed to increase from these extremely low values (Fig. 4), which has been interpreted to represent the proliferation of cyanobacterial oxygenic photosynthesis (Eigenbrode and Freeman, 2006). Cyanobacterial oxygen production would presumably have increased oxidant availability in the water column, perhaps accompanied by a rise in atmospheric redox potential (Pavlov et al., 2001; Claire et al., 2006; Kurzweil et al., 2013). This inference of local oxidation is supported by the $\delta^{34}S$–$\Delta^{33}S$ trends shown in microbialite facies by Zerkle et al. (2012), as well as trace metal systematics from the Griqualand West basin (Kendall et al., 2010; Czaja et al., 2012). The increase in background $\delta^{13}C_{org}$ is observed to be synchronous with the increase in S-MIF magnitude, and potentially a broad scale shift toward shallower $\Delta^{36}S/\Delta^{33}S$ slopes (~ −0.9), indicating a coupling between the biosphere and the evolution of Earth's atmospheric composition in the early Neoarchaean.

Following the evolution of oxygenic photosynthesis, Archaean ecosystem models predict fluxes of oxygen and methane in a roughly 2:1 stoichiometric ratio, albeit at much lower levels of total primary productivity (Kasting et al., 2001; Kharecha et al., 2005; Canfield, 2005; Catling and Claire, 2005). The net effect of enhanced fluxes of oxygen and methane into reducing model atmospheres depends on the amount of other reducing species present, in particular volcanogenic hydrogen or methane derived from serpentinisation. Kurzweil et al. (2013) and Claire et al. (2014) present model atmospheres in which the proliferation of oxygenic photosynthesis (and associated plausible methane fluxes) could first clear an assumed pre-existing haze, causing an evolution to a stable haze-free atmospheric state. Depending on the assumptions regarding the background redox state, further modelled enhancements of primary productivity could lead to either the formation of another, more oxygen-rich, photochemical haze (Kurzweil et al., 2013) or to a rise in atmospheric oxygen (Claire et al., 2014). In all but the latter case, the model atmospheres remain strongly reducing, with pO_2 reaching a maximum of $\sim 10^{-7}$ PAL in the atmospheric boundary layer near the source of primary productivity (Olson et al., 2013; Claire et al., 2014). Consequently, the increase in S-MIF magnitude, and putative decrease in $\Delta^{36}S/\Delta^{33}S$ slopes at 2.71–2.73 Ga, could be explained by subtle increases in atmospheric redox potential, driven by photosynthetically enhanced fluxes of oxygen and methane (Zerkle et al., 2012; Kurzweil et al., 2013; Claire et al., 2014). Taken together, these data and models provide some credence to the suggestion of increased availability of near-surface O_2 prior to the GOE (e.g., Anbar et al., 2007; Wille et al., 2007; Frei et al., 2009; Kendall et al., 2010; Thomazo et al., 2011). Importantly, however, these simulations only show subtle increases in atmospheric redox potential ($pO_2 \approx$

10^{-9}–10^{7} PAL) at the ground level, with extremely reducing conditions persisting throughout most of the troposphere (Claire et al., 2014), as testified by the continued preservation of S-MIF (Figs. 2–4). This apparent model-data discrepancy may be better resolved via the recent suggestion that localised benthic and soil environments housed oxidative-weathering reactions in profound redox disequilibrium with the atmosphere, supplying trace elements to the oceans without a corresponding major leak of O_2 to the atmosphere (Lalonde and Konhauser, 2015).

5.2. What drove atmospheric evolution in the prelude to the GOE?

In our attempts to delineate the operation of the terminal-Neoarchaean (~2.7–2.5 Ga) atmosphere we find multiple C–S anomalies where $\Delta^{36}S/\Delta^{33}S$ slopes temporarily steepen in association with extremely low $\delta^{13}C_{Org}$ values. These trends are observed both within our new data and upon closer examination of previously published records (Zerkle et al., 2012), demonstrating that they are spatially and temporally widespread, implying repeated oscillatory changes from the assumed dominant post-2.7 Ga haze-free atmospheric state.

Given that the C–S anomalies feature similar $\Delta^{36}S/\Delta^{33}S$ slopes (~ -1.5) to some pre-2.7 Ga sediments (Kurzweil et al., 2013), it is tempting to draw parallels between the two time periods, and speculate that the atmosphere regressed toward a reduced state, resembling that prior to the proliferation of oxygenic photosynthesis. However, we hypothesise that the Neoarchaean hazes captured during the 2.7–2.5 Ga C–S anomalies ($\Delta^{36}S/\Delta^{33}S \sim -1.5$ with *high* magnitude $\Delta^{36}S$ and $\Delta^{33}S$) represent a different atmospheric state than the putative pre-2.7 Ga haze ($\Delta^{36}S/\Delta^{33}S$ slope of -1.5 with *low* magnitude $\Delta^{36}S$ and $\Delta^{33}S$). Support for the existence of separate hazy atmospheric states pre- and post-photosynthesis can again be found in 1D photochemical models, which demonstrate that post-photosynthetic hazy regimes display a greater variety of sulphur exit channels, potentially explaining the observed difference in S-MIF magnitudes (Zerkle et al., 2012; Kurzweil et al., 2013; Claire et al., 2014). Within this conceptual framework, enhanced biogenic oxygen and methane fluxes, with the concomitant formation of an organic-rich haze, seemingly has the potential to simultaneously affect both $\Delta^{36}S/\Delta^{33}S$ and $\delta^{13}C_{Org}$ as observed, requiring only a proposed mechanism for the necessary pulses in productivity.

Kurzweil et al. (2013) argued that the rapid and long-term atmospheric rearrangement witnessed at 2.73–2.71 Ga was best explained by biological innovation (i.e., the proliferation of oxygenic photosynthesis) rather than by any single geological process. While we question the unidirectional change as discussed by Kurzweil et al. (2013), our interpretation does require the presence of oxygen-producing organisms but is incompatible with a single evolutionary event, instead requiring a repeated or transitory driver. We hypothesise that episodic amplification of biogenic methane fluxes could have occurred if a background state of major or trace nutrient limitation was periodically overcome via tectonics, enhanced weathering fluxes and/or heightened submarine hydrothermal emanations (e.g., Anbar et al., 2007). Under this scenario, enhanced biogenic methane fluxes could have preceded either by a top down stimulation of the biosphere, where increased availability of organic matter resulting from enhanced primary productivity drove methanogenesis, or through selective stimulation of methanogens via supply of previously limited essential metals (e.g., Konhauser et al., 2009). The heightened flux of methane could then have increased the atmospheric CH_4:CO_2 mixing ratio, leading to the development of a temporary hydrocarbon haze. This new hazy atmospheric state could conceivably have been maintained until the additional nutrient supply had been depleted, causing biogenic gas fluxes to return to their background state, resulting in a relaxation towards the haze-free background state.

Ultimately, testing and discriminating between these causative mechanisms will require higher resolution sulphur- and carbon-isotope records coupled with additional nutrient (e.g., trace metals) profiles, as informed by our core-wide records. These new datasets could reveal crucial details concerning the timing and structure of the C–S anomalies, and inform on the causes/consequences of the repeated terminal-Neoarchaean atmospheric oscillations. Coupling our data with emerging experimental data and next generation S-MIF-predictive photochemical models would also permit a more detailed interpretation of the Archaean atmospheric composition beyond the lack of oxygen and ozone. Furthermore, the statistically significant changes to shallower $\Delta^{33}S/\Delta^{36}S$ of ~ -0.6, may represent a further distinct, as yet un-interpreted, state for atmospheric chemistry, which is ripe for further integrated experimental, geochemical, and numerical studies (e.g. Oduro et al., 2014).

6. Conclusions

The original notion of a dynamic bistable Neoarchaean atmosphere, oscillating between a hazy state fuelled by photochemical polymerisation of methane and a haze-free background, was based on analyses of sediments from a single core (Zerkle et al., 2012; Farquhar et al., 2013). We set out to test this hypothesis by extending the search for the relevant chemostratigraphic trends in other coeval carbon- and sulphur-isotopic records. Our new data indicate 2 correlative C–S anomalies from geographically widespread sedimentary successions along with at least 2 other C–S anomalies, strengthening the hypothesised link between the Neoarchaean atmospheric sulphur cycle and the marine carbon cycle (Zerkle et al., 2012).

Strata older than ~2.7 Ga feature low magnitude S-MIF, characterised by variable $\Delta^{36}S/\Delta^{33}S$ slopes. Strata younger than ~2.7 Ga feature $\Delta^{36}S/\Delta^{33}S$ slopes closer to -0.9 associated with high magnitude S-MIF, with periodic oscillations toward steeper $\Delta^{36}S/\Delta^{33}S$ slopes and low $\delta^{13}C_{Org}$. These data require a complex and long-term evolution of atmospheric chemistry, which could be explained by changing biospheric productivity perturbing the atmospheric redox state to alter the dominant S-MIF formation reactions and the relative importance of sulphur atmospheric exit channels.

The presence of C–S anomalies between ~2.7–2.5 Ga preserved in multiple, spatially separated, sedimentary successions is consistent with a periodically hazy atmosphere during this time period. Consequently, this work serves to substantiate previous claims, whilst demonstrating that the terminal-Neoarchaean atmosphere was more chemically dynamic than previously recognised.

Although there is a paucity of high resolution coupled carbon- and sulphur-isotope datasets, it is intriguing to note that these aberrations appear to be crucial events in the overture to the GOE, representing a time in Earth's history where biology apparently tightly regimented atmosphere chemistry over short timescales. We speculate that enhanced nutrient availability (e.g., organic carbon or trace metals), derived from either heightened hydrothermal or weathering fluxes, facilitated the proliferation of the biosphere, thus amplifying global biogenic methane and oxygen fluxes. Mechanistic uncertainties notwithstanding, these repeated chemical oscillations suggest a terminal-Neoarchaean coupling between biogenic gas fluxes and atmospheric photochemistry. Somewhat counter-intuitively, Neoarchaean atmospheric models produce more reduced hazy conditions under some conditions of coupled oxygen and methane production (Kurzweil et al., 2013; Zerkle et al., 2012; Claire et al., 2014). Accordingly, these new records emphasise the need to understand the mechanisms and feedbacks controlling both biogenic oxygen *and* methane fluxes in the pre-

lude to the GOE, whilst demonstrating the need for increasingly higher resolution, more precise, chemostratigraphic records, in order to more fully understand the ensuing planetary oxygenation.

Acknowledgements

We thank A. Czaja, K. Freeman and the staff at the South African National Core Library in Donkerhoek for facilitating access to the core materials, C. Jones and K. Moulton for assistance with sampling and rock crushing, and E. Stüeken for the provision of the $\Delta^{3x}S$ database. G.I. thanks C.L. Holmes for comments on earlier versions of the manuscript and C.S. Miller for assistance with drafting some of the artwork. This work benefited from careful reviews by Colin Goldblatt and Bozwell Wing and the editorial oversight of Bernard Marty. This study was supported financially by NERC Fellowship NE/H016805/2 (to A.Z.) and a NERC Standard Grant NE/J023485/2 (to A.Z., M.C. and S.P.), along with a SAGES Postdoctoral & Early Career Researcher Exchange grant to G.I.

Appendix A. Supplementary material

Supplementary material related to this article can be found online at http://dx.doi.org/10.1016/j.epsl.2015.09.018.

References

Altermann, W., Nelson, D.R., 1998. Sedimentation rates, basin analysis and regional correlations of three Neoarchaean and Palaeoproterozoic sub-basins of the Kaapvaal craton as inferred from precise U–Pb zircon ages from volcaniclastic sediments. Sediment. Geol. 120, 225–256.

Altermann, W., Siegfried, H.P., 1997. Sedimentology and facies development of an Archaean shelf: carbonate platform transition in the Kaapvaal Craton, as deduced from a deep borehole at Kathu, South Africa. J. Afr. Earth Sci. 24, 391–410.

Anbar, A.D., Duan, Y., Lyons, T.W., Arnold, G.L., Kendall, B., Creaser, R.A., Kaufman, A.J., Gordon, G.W., Scott, C., Garvin, J., Buick, R., 2007. A whiff of oxygen before the great oxidation event? Science 317, 1903–1906.

Bekker, A., Holland, H.D., Wang, P.L., Rumble, D., Stein, H.J., Hannah, J.L., Coetzee, L.L., Beukes, N.J., 2004. Dating the rise of atmospheric oxygen. Nature 427, 117–120.

Beukes, N.J., 1987. Facies relations, depositional environments and diagenesis in a major early Proterozoic stromatolitic carbonate platform to basinal sequence, Campbellrand Supgroup, Transvaal Supergroup, southern Africa. Sediment. Geol. 54, 1–46.

Blake, T.S., 1993. Late Archaean crustal extension, sedimentary basin formation, flood basalt volcanism and continental rifting: the Nullagine and Mount Jope Supersequences, Western Australia. Precambrian Res. 60, 185–241.

Blake, T.S., Buick, R., Brown, S.J.A., Barley, M.E., 2004. Geochronology of a Late Archaean food basalt province in the Pilbara Craton, Australia: constraints on basin evolution, volcanic and sedimentary accumulation, and continental drift rates. Precambrian Res. 133, 143–173.

Blockley, J.G., Tehnas, I.J., Mandyczewsky, A., Morris, R.C., 1993. Proposed Stratigraphic Subdivisions of the Marra Mamba Iron Formation and the Lower Wittenoom Dolomite, Hamersley Group, Western Australia. Report 34. Geological Survey of Western Australia, pp. 47–63.

Button, A., 1973. The stratigraphic history of the Malmani dolomite in the eastern and north-eastern Transvaal. Verh. Geol. Ver. S.-Afr. 76, 229–247.

Cabral, R.A., Jackson, M.G., Rose-Koga, E.F., Koga, K.T., Whitehouse, M.J., Antonelli, M.A., Farquhar, J., Day, J.M.D., Hauri, E.H., 2013. Anomalous sulphur isotopes in plume lavas reveal deep mantle storage of Archaean crust. Nature 496, 490–493.

Canfield, D.E., 2005. The early history of atmospheric oxygen: homage to Robert M. Garrels. Annu. Rev. Earth Planet. Sci. 33, 1–36.

Canfield, D.E., Raiswell, R., Westrich, J.T., Reaves, C.M., Berner, R.A., 1986. The use of chromium reduction in the analysis of reduced inorganic sulfur in sediments and shales. Chem. Geol. 54, 149–155.

Catling, D.C., Claire, M.W., 2005. How Earth's atmosphere evolved to an oxic state: a status report. Earth Planet. Sci. Lett. 237, 1–20.

Claire, M.W., Catling, D.C., Zahnle, K.J., 2006. Biogeochemical modelling of the rise in atmospheric oxygen. Geobiology 4, 239–269.

Claire, M.W., Kasting, J.F., Domagol-Goldman, Buick R, S., Stuëken, E., Meadows, V., 2014. Modeling the signature of sulfur mass-independent fractionation produced in the Archean atmosphere. Geochim. Cosmochim. Acta 141, 365–380.

Czaja, A.D., Johnson, C.M., Beard, B.L., Eigenbrode, J.L., Freeman, K.H., Yamaguchi, K.E., 2010. Iron and carbon isotope evidence for ecosystem and environmental diversity in the 2.7 to 2.5 Ga Hamersley Province, Western Australia. Earth Planet. Sci. Lett. 292, 170–180.

Czaja, A.D., Johnson, C.M., Roden, E.E., Beard, B.L., Voegelin, A.R., Nagler, T.F., Beukes, N.J., Wille, W., 2012. Evidence of free oxygen in the Neoarchean ocean based on coupled iron-molybdenum fractionation. Geochim. Cosmochim. Acta 86, 118–137.

Danielache, S.O., Hattori, S., Johnson, M.S., Ueno, Y., Nanbu, S., Yoshida, N., 2012. Photoabsorption cross-section measurements of ^{32}S, ^{33}S, ^{34}S, and ^{36}S sulfur dioxide for the B^1B_1–X^1A_1 absorption band. J. Geophys. Res., Atmos. 177. http://dx.doi.org/10.1029/2012JD017464.

Domagal-Goldman, S.D., Kasting, J.F., Johnston, D.T., Farquhar, J., 2008. Organic haze, glaciations and multiple sulfur isotopes in the Mid-Archean Era. Earth Planet. Sci. Lett. 269, 29–40.

Eigenbrode, J.L., Freeman, K.H., 2006. Late Archean rise of aerobic microbial ecosystems. Proc. Natl. Acad. Sci. USA 103, 15759–15764.

Eigenbrode, J.L., Freeman, K.H., Summons, R.E., 2008. Methylhopane biomarker hydrocarbons in Hamersley Province sediments provide evidence for Neoarchean aerobiosis. Earth Planet. Sci. Lett. 273, 323–331.

Eriksson, P.G., Altermann, W., Hartzer, F.J., 2006. The Transvaal supergroup and its precursors. In: Johnson, M.R., Anhaeusser, C.R., Thomas, R.J. (Eds.), Geology of South Africa. Geological Society of South Africa/Ouncil for Geoscience, Johannesburg/Petoria, pp. 237–260.

Farquhar, J., Bao, H., Thiemens, M., 2000. Atmospheric influence of Earth's earliest sulfur cycle. Science 289, 756–758.

Farquhar, J., Savarino, J., Airieau, S., Thiemens, M.H., 2001. Observation of wavelength-sensitive mass-independent sulfur isotope effects during SO_2 photolysis: implications for the early atmosphere. J. Geophys. Res., Planets 106, 32829–32839.

Farquhar, J., Peters, M., Johnston, D.T., Strauss, H., Masterson, A., Wiechert, U., Kaufman, A.J., 2007. Isotopic evidence for Mesoarchaean anoxia and changing atmospheric sulphur chemistry. Nature 449, 706–709.

Farquhar, J., Zerkle, A.L., Bekker, A., 2011. Geological constraints on the origin of oxygenic photosynthesis. Photosynth. Res. 107, 11–36.

Farquhar, J., Cliff, J., Zerkle, A.L., Kamyshny, A., Poulton, S.W., Claire, M., Adams, D., Harms, B., 2013. Pathways for Neoarchean pyrite formation constrained by mass-independent sulfur isotopes. Proc. Natl. Acad. Sci. USA 110, 17638–17643.

Farquhar, J., Zerkle, A.L., Bekker, A., 2014. Geologic and geochemical constraints on the Earth's early atmosphere. In: Holland, H., Turekian, K. (Eds.), The Atmosphere – History, 2nd ed. In: Treatise on Geochemistry, vol. 6. Elsevier, Oxford, pp. 91–138.

Fischer, W.W., Schroeder, S., Lacassie, J.P., Beukes, N.J., Goldberg, T., Strauss, H., Horstmann, U.E., Schrag, D.P., Knoll, A.H., 2009. Isotopic constraints on the Late Archean carbon cycle from the Transvaal Supergroup along the western margin of the Kaapvaal Craton, South Africa. Precambrian Res. 169, 15–27.

Francisco, J.S., Lyons, J.R., Williams, I.H., 2005. High-level ab-initio studies of the structure, vibrational spectra and energetics of S_3. J. Phys. Chem. 123, 054302.

Frei, R., Gaucher, C., Poulton, S.W., Canfield, D.E., 2009. Fluctuations in Precambrian atmospheric oxygen recorded by chromium Isotopes. Nature 461, 250–254.

Guo, Q., Strauss, H., Kaufman, A.J., Schröder, S., Gutzmer, J., Wing, B., Baker, M.A., Bekker, A., Jin, Q., Kim, S.T., Farquhar, J., 2009. Reconstructing Earth's surface oxidation across the Archean–Proterozoic transition. Geology 37, 399–402.

Halevy, I., 2013. Production, preservation, and biological processing of mass-independent sulfur isotope fractionation in the Archean surface environment. Proc. Natl. Acad. Sci. USA 110, 17644–17649.

Haqq-Misra, J.D., Domagal-Goldman, S.D., Kasting, P.J., Kasting, J.F., 2008. A revised, hazy methane greenhouse for the Archean Earth. Astrobiology 8, 1127–1137.

Holland, H.D., 2006. The oxygenation of the atmosphere and oceans. Philos. Trans. R. Soc. Lond. B, Biol. Sci. 361, 903–915.

Johnston, D.T., 2011. Multiple sulfur isotopes and the evolution of Earth's surface sulfur cycle. Earth-Sci. Rev. 106, 161–183.

Kasting, J.F., Pavlov, A.A., Siefert, J.L., 2001. A coupled ecosystem–climate model for predicting the methane concentration in the Archean atmosphere. Orig. Life Evol. Biosph. 31, 271–285.

Kendall, B., Reinhard, C.T., Lyons, T.W., Kaufman, A.J., Poulton, S.W., Anbar, A.D., 2010. Pervasive oxygenation along late Archaean ocean margins. Nat. Geosci. 3, 647–652.

Kharecha, P., Kasting, J.F., Siefert, J., 2005. A coupled atmosphere–ecosystem model of the early Earth. Geobiology 3, 53–76.

Knoll, A.H., Beukes, N.J., 2009. Introduction: initial investigations of a Neoarchean shelf margin-basin transition (Transvaal Supergroup, South Africa). Precambrian Res. 169, 1–14.

Konhauser, K.O., Pecoits, E., Lalonde, S.V., Papineau, D., Nisbet, E.G., Barley, M.E., Arndt, N.T., Zahnle, K., Kamber, B.S., 2009. Oceanic nickle depletion and a methanogen famine before the Great Oxidation Event. Nature 458, 750–754.

Kurzweil, F., Claire, M., Thomazo, C., Peters, M., Hannington, M., Strauss, H., 2013. Atmospheric sulfur rearrangement 2.7 billion years ago: evidence for oxygenic photosynthesis. Earth Planet. Sci. Lett. 366, 17–26.

Lalonde, S.V., Konhauser, K.O., 2015. Bethic perspective on Earth's oldest evidence for oxygenic photosynthesis. Proc. Natl. Acad. Sci. USA 112, 995–1000.

Lascelles, D.F., 2000. Marra Mamba Iron formation stratigraphy in the eastern chichester Range, Western Australia. Aust. J. Earth Sci. 47, 799–806.

Lawrence, S.D., 1985. Final report on exploration completed within exploration license EL 47/104, Billadunna Spring, Pyramid, Western Australia. CRA Exploration

Pty Ltd unpublished report. Item 3189. Western Australia Geological Survey open file.
Masterson, A.L., Farquhar, F., Wing, B.A., 2011. Sulfur mass-independent fractionation patterns in the broadband UV photolysis of sulfur dioxide: pressure and third body effects. Earth Planet. Sci. Lett. 306, 253–260.
Meakins, A.L., 1987. CRA Exploration Pty. Ltd. final report on exploration completed within the Mulga Project area, Mt. Bruce 1:250 000 sheet, Pilbara region, Western Australia. Item 3458. Western Australia Geological Survey open file.
Miyano, T., Beukes, N.J., 1984. Phase relations of stilpnomelane, ferri-annite, and riebeckite in very low grade metamorphosed iron formations. Verh. Geol. Ver. S.-Afr. 87, 111–124.
Oduro, H., Kamyshny Jr, A., Guo, W., Farquhar, J., 2011a. Multiple sulfur isotope analysis of volatile organic sulfur compounds and their sulfonium precursors in coastal marine environments. Mar. Chem. 124, 78–89.
Oduro, H.D., Harms, B., Sintim, H.O., Kaufman, A.J., Cody, G., Farquhar, J., 2011b. Evidence of magnetic isotope effects during thermochemical sulfate reduction. Proc. Natl. Acad. Sci. USA 108, 17635–17638.
Oduro, H., Izon, G., Ono, S., 2014. Mass-dependent and Mass-independent Sulphur Isotope Fractionation Accompanying Thermal- and Photo-chemical Decomposition of Sulphur Bearing Organic Compounds. Geophysical Research Abstracts, 16, EGU2014-14036-1: EGU General Assembly, Vienna.
Ohmoto, H., Watanabe, Y., Ikemi, H., Poulson, S.R., Taylor, B.E., 2006. Sulphur isotope evidence for an oxic Archaean atmosphere. Nature 442, 908–911.
Olson, S.L., Kump, L.R., Kasting, J.F., 2013. Quantifying the areal extent and dissolved oxygen concentrations of Archean oxygen oases. Chem. Geol. 362, 35–43.
Ono, S., Eigenbrode, J.L., Pavlov, A.A., Kharecha, P., Rumble, D., Kasting, J.F., Freeman, K.H., 2003. New insights into Archean sulfur cycle from mass-independent sulfur isotope records from the Hamersley Basin, Australia. Earth Planet. Sci. Lett. 213, 15–30.
Ono, S., Beukes, N.J., Rumble, D., Fogel, M., 2006a. Early evolution of the Earth's atmospheric oxygen from multiple-sulfur and carbon isotope records of the 2.9 Ga Pongola Supergroup, Southern Africa. S. Afr. J. Geol. 109, 97–108.
Ono, S., Wing, B., Johnston, D., Farquhar, J., Rumble, D., 2006b. Mass-dependent fractionation of quadruple stable sulfur isotope system as a new tracer of sulfur biogeochemical cycles. Geochim. Cosmochim. Acta 70, 2238–2252.
Ono, S., Beukes, N.J., Rumble, D., 2009. Origin of two distinct multiple-sulfur isotope compositions of pyrite in the 2.5 Ga Klein Naute Formation, Griqualand West Basin, South Africa. Precambrian Res. 169, 48–57.
Pavlov, A.A., Kasting, J.F., 2002. Mass-Independent fractionation of sulphur isotopes in Archean sediments: strong evidence for an anoxic Archean atmosphere. Astrobiology 2, 27–41.
Pavlov, A.A., Kasting, J.F., Eigenbrode, J.L., Freeman, K.H., 2001. Organic haze in the Earths early atmosphere: low-^{13}C Late Archean kerogens? Geology 29, 1003–1006.
Penniston-Dorland, S.C., Wing, B.A., Nex, P.A.M., Kinnaird, J.A., Farquhar, J., Brown, M., Sharman, E.R., 2008. Multiple sulfur isotopes reveal a primary magmatic origin for the Platreef PGE deposit, Bushveld Complex, South Africa. Geology 36, 979–982.
Richards, M.N., 1985. CRA Exploration Pty. Ltd. final report on exploration completed within exploration licenses Ripon Hills North 45/63, Ripon Hills South 45/64 and Gingarrigan Creek 45/65, Nullagine, S F 51-5, Western Australia. Item 2655. Western Australia Geological Survey open file.
Schröder, S., Lacassie, J.P., Beukes, N.J., 2006. Stratigraphic and geochemical framework of the Agouron drill cores, Transvaal Supergroup (Neoarchean-Paleoproterozoic, South Africa). S. Afr. J. Geol. 109, 23–54.
Simonson, B.M., Schubel, K.A., Hassler, S.W., 1993. Carbonate sedimentology of the Early Precambrian Hamersley Group of Western–Australia. Precambrian Res. 60, 287–335.
Smith, R.E., Perdrix, J.L., Parks, T.C., 1982. Burial metamorphism in the Hamersley Basin, Western Australia. J. Petrol. 23, 75–102.
Stüeken, E.E., Catling, D.C., Buick, R., 2012. Contributions to late Archaean sulphur cycling by life on land. Nat. Geosci. 5, 722–725.
Sumner, D.Y., Beukes, N.J., 2006. Sequence stratigraphic development of the Neoarchean Transvaal carbonate platform, Kaapvaal Craton, South Africa. S. Afr. J. Geol. 109, 11–22.
Thomazo, C., Ader, M., Farquhar, J., Philippot, P., 2009. Methanotrophs regulated atmospheric sulfur isotope anomalies during the Late Archean (Tumbiana Formation, Western Australia). Earth Planet. Sci. Lett. 279, 65–75.
Thomazo, C., Ader, M., Philippot, P., 2011. Extreme ^{15}N-enrichments in 2.72-Gyr-old sediments: evidence for a turning point in the nitrogen cycle. Geobiology 9, 107–120.
Thomazo, C., Nisbet, E.G., Grassineau, N.V., Peters, M., Strauss, H., 2013. Multiple sulfur and carbon isotope composition of sediments from the Belingwe Greenstone Belt (Zimbabwe): a biogenic methane regulation on mass independent fractionation of sulfur during the Neoarchean? Geochim. Cosmochim. Acta 121, 120–138.
Thorne, A.M., Trendall, A.F., 2001. Geology of the Fortescue Group, Pilbara Craton, Western Australia. Bulletin 144. Geological Survey of Western Australia, 249 pp.
Trendall, A.F., Blockley, J.G., 1970. The Iron Formations of the Precambrian Hamersley Group, Western Australia. Bulletin 119. Geological Survey of Western Australia, 366 pp.
Ueno, Y., Johnson, M.S., Danielache, S.O., Eskebjerg, C., Pandey, A., Yoshida, N., 2009. Geological sulfur isotopes indicate elevated OCS in the Archean atmosphere, solving faint young sun paradox. Proc. Natl. Acad. Sci. USA 106, 14784–14789.
Whitehill, A.R., Ono, S., 2012. Excitation band dependence of sulfur isotope mass-independent fractionation during photochemistry of sulfur dioxide using broadband light sources. Geochim. Cosmochim. Acta 94, 238–253.
Whitehill, A.R., Xie, C., Xixi Hu, X., Xie, D., Guo, H., Ono, S., 2013. Vibronic origin of sulfur mass-independent isotopes effect in photoexcitation of SO_2 and the implications to the early earth's atmosphere. Proc. Natl. Acad. Sci. USA 110, 17697–17702.
Wille, M., Kramers, J.D., Nägler, T.F., Beukes, N.J., Schroeder, S., Meisel, Th., Lacassie, J.P., Voegelin, A.R., 2007. Evidence for a gradual rise of oxygen between 2.6 and 2.5 Ga from Mo isotopes and Re-PGE signatures. Geochim. Cosmochim. Acta 71, 2417–2435.
Zerkle, A.L., Claire, M.W., Domagal-Goldman, S.D., Farquhar, J., Poulton, S.W., 2012. A bistable organic-rich atmosphere on the Neoarchaean Earth. Nat. Geosci. 5, 359–363.